APPLIED PHYSICS LETTERS **111**, 073102 (2017)

Terahertz spectroscopy of an electron-hole bilayer system in AlN/GaN/AlN quantum wells

H. Condori Quispe,[1,a)] S. M. Islam,[2,a)] S. Bader,[2] A. Chanana,[1] K. Lee,[2] R. Chaudhuri,[2] A. Nahata,[1] H. G. Xing,[2,3] D. Jena,[2,3] and B. Sensale-Rodriguez[1]
[1]*Department of Electrical and Computer Engineering, University of Utah, Salt Lake City, Utah 84112, USA*
[2]*School of Electrical and Computer Engineering, Cornell University, Ithaca, New York 14853, USA*
[3]*Department of Materials Science and Engineering, Cornell University, Ithaca, New York 14853, USA*

(Received 12 May 2017; accepted 18 July 2017; published online 15 August 2017)

We report studies on the nanoscale transport dynamics of carriers in strained AlN/GaN/AlN quantum wells: an electron-hole bilayer charge system with a large difference in transport properties between charge layers. From electronic band diagram analysis, the presence of spatially separated two-dimensional electron and hole charge layers is predicted at opposite interfaces. Since these charge layers exhibit distinct spectral signatures at terahertz frequencies, a combination of terahertz and far-infrared spectroscopy enables us to extract (a) individual contributions to the total conductivity and (b) effective scattering rates for charge-carriers in each layer. Furthermore, by comparing direct-current and THz-extracted conductivity levels, we are able to determine the extent to which structural defects affect charge transport. Our results evidence that (i) a non-unity Hall-factor and (ii) the considerable contribution of holes to the overall conductivity lead to a lower apparent mobility in Hall-effect measurements. Overall, our work demonstrates that terahertz spectroscopy is a suitable technique for studying bilayer charge systems with large differences in transport properties between layers such as quantum wells in III-nitride semiconductors. *Published by AIP Publishing.*
[http://dx.doi.org/10.1063/1.4996925]

III-V compound semiconductors based on gallium nitride (GaN) have emerged as one of the most attractive materials for power electronics owing to their large bandgap ($\sim$3.4 eV), breakdown field ($\sim$3 MV/cm), and ability to operate at high frequencies, and, thus, remain the subject of intense research over the past several decades.[1,2] GaN showcases excellent properties such as large peak electron velocity ($\sim 2.5 \times 10^7$ cm/s), large saturation velocity ($\sim 2.0 \times 10^7$ cm/s), and excellent carrier transport properties as evidenced by a high electron mobility ($\mu > 2400\,\mathrm{cm^2/V\,s}$) in GaN two-dimensional electron gases (2DEGs); these properties make GaN suitable for use as a channel material in high frequency power devices.[3] In addition, aluminum nitride (AlN) withstands high temperature and high power density, owing to its very large band gap ($\sim$6.2 eV) and high thermal conductivity ($\sim$340 W/m K), among other properties.[4] AlN/GaN/AlN quantum wells (QWs), i.e., thin GaN layers surrounded by AlN buffer and barrier layers, bring together all the above-mentioned features as an attractive platform for electronic applications. In this regard, QW devices can provide tight electrostatic control and quantum confinement of charge carriers, thereby preventing degradation in performance by short-channel effects. Moreover, the superior thermal conductivity of AlN enables excellent heat dissipation.

A series of recent reports experimentally demonstrated the feasibility of ultra-thin GaN QWs surrounded by AlN buffer and barrier layers.[5–7] The discontinuity in spontaneous and piezoelectric polarization at the two heterojunctions of the QW gives rise to highly charged regions near the boundaries. Mobile carriers concentrate at these interfaces forming two-dimensional (2D) charge gases. Simulations predict that a population of distinct carrier species exists at each interface, i.e., in the upper interface, a 2DEG is formed, whereas at the bottom interface, a 2D hole gas (2DHG) is formed.[5,6] Often, electrical characterization of these complex electron-hole bilayer systems is performed via Hall-effect measurements. While conventional Hall-effect measurements provide a weighted average of the electron-hole bilayer system mobility and charge concentration, a more careful transport analysis is required to identify the individual effects of each type of carrier. In this work, we are able to decouple the electron and hole transport properties in this system by means of non-contact terahertz spectroscopy. A unique aspect of this approach is that the nanoscale transport properties, i.e., *conductivity and scattering rates*, for electron and hole layers can be independently extracted; this results from the distinct spectral features arising from each carrier species upon the interaction with terahertz electromagnetic radiation. Our results evidence that the relatively modest electron mobility extracted from Hall-effect measurements ($\mu < 400\,\mathrm{cm^2/V\,s}$) is not the result of structural defects such as dislocations but likely the consequence of (i) a non-unity Hall-factor and (ii) the effect of holes, which due to their considerable contribution to the overall conductivity substantially reduce the apparent Hall mobility. In effect, relaxation times of the 2DEGs associated with a drift mobility of $\sim 1000\,\mathrm{cm^2/V\,s}$ are consistently observed across all the analyzed samples. Overall, our results demonstrate an alternative, simple, yet insightful method to probe for the carrier transport properties in this bilayer system, which enables us to characterize (*a*) *the contributions of electron and hole layers to the overall conductivity*, (*b*) *the effective scattering rates for*

[a)]H. Condori Quispe and S. M. Islam contributed equally to this work.

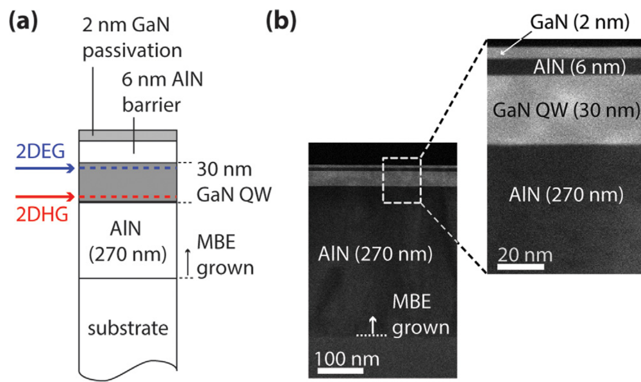

FIG. 1. (a) Schematic cross section of the analyzed QWs. (b) TEM image of a representative QW under study.

electrons and holes, and (*c*) *the extent to which structural effects affect the overall conductivity*.

The schematic cross section of the analyzed heterostructures is shown in Fig. 1(a), which consists of a thick ~270 nm unintentionally doped AlN buffer layer, followed by a ~30 nm GaN layer to host the 2DEG channel, a 6 nm AlN barrier, and a 2 nm GaN passivation cap layer. Three different substrates were employed to support the QW structures and can be grouped into three sets: *Sample Set #1* utilized a 6H SiC substrate with a thickness of $d_{S1} = 375\,\mu$m; *Sample Set #2* utilized a AlN template with a thickness of $d_{S2a} = 1\,\mu$m on a sapphire substrate with a thickness of $d_{S2b} = 430\,\mu$m; and *Sample Set #3* utilized a bulk AlN substrate of $d_{S3} = 550\,\mu$m. In all three sample sets, the QW heterostructures were grown using a Veeco Gen 930 plasma-assisted MBE system. Additional details about the growth conditions are discussed elsewhere.[5,7] The schematic cross section of the QWs was examined by transmission electron microscopy (TEM). Figure 1(b) shows the cross-sectional TEM image of a representative GaN QW heterostructure. The carrier concentration and mobility were obtained from Hall-effect measurements across all samples; the extracted electrical transport properties are listed on the first three columns of Table I. All measurements reported in this work were performed at room temperature. The four samples in *Sample Set #1*, corresponding to different nucleation conditions of the buffer AlN layers such as Nitrogen rich (*S1a*), migration enhanced epitaxy (*S1b*), Gallium surfactant mediated (*S1c*), and short period super-lattice (*S1d*) growth conditions, exhibited Hall mobilities (μ_{Hall}) of 366, 250, 359, and 290 cm^2/V s, respectively, with charge densities (n_s) ranging between 2.81 and 4.78×10^{13} cm^{-2}. The samples in *Sample Set #2* and #3 showed charge densities of 3.20 and 4.31×10^{13} cm^{-2} but lower Hall mobilities of 94 and 153 cm^2/V s, respectively. We attribute the lower mobility observed in *Sample Sets #2* and *#3* to defects generated during un-optimized nucleation on the AlN surfaces.[5]

In order to provide insights into the carrier distributions in the QWs, we numerically calculated the energy band diagrams for the active region, as shown in Fig. 2(a); see the supplementary material for further details.

To model the effect of free carrier dynamics on the terahertz transmission through the samples, the 2DEG/2DHG conductivities were modeled using a Drude frequency dispersion.[8] This assumption is further validated via measurements through GaN control samples containing just one charge carrier species, i.e., only electrons or holes. Our results evidence that both electrons and holes are indeed characterized by Drude responses with single scattering times (supplementary material). Since the thickness of the QW is negligible compared to the wavelength of the terahertz radiation, the system can be modeled via an effective (bilayer) conductivity given by the sum of the electron and hole layer conductivities[9]

$$\sigma_b(\omega) = \sigma_e^0/(1 + j\omega\tau_e) + \sigma_h^0/(1 + j\omega\tau_h), \qquad (1)$$

where $\sigma_b(\omega)$ is the bilayer dynamic conductivity, σ_e^0 is the zero-frequency dynamic conductivity of the 2DEG, τ_e is the momentum relaxation time for electrons in the 2DEG, σ_h^0 is the zero-frequency dynamic conductivity of the 2DEG, τ_h is the 2DHG momentum relaxation time, and ω is the angular frequency. Figure 2(b) shows the calculated bilayer conductivity following Eq. (1) and assuming 2DEG and 2DHG direct-current (DC) conductivities of 1 and 0.1 mS and momentum relaxation times of 160 and 10 fs, respectively, which correspond to typical values reported in the literature.[5,10] These relaxation times are in the range of those observed in the control samples (see Fig. S2 in the supplementary material). As depicted in Fig. 2(b), two distinct frequency windows can be identified: (*i*) below ~3 THz, where both electrons and holes contribute to the overall conductivity, and (*ii*) above ~3 THz, which is beyond the 2DEG Drude roll-off and thus the overall conductivity is set mainly by the 2DHG.

We used two different terahertz systems to characterize the samples: a continuous wave (CW) terahertz spectrometer and a terahertz time-domain spectrometer (THz-TDS). The CW spectrometer (TOPTICA Photonics) used InGaAs photomixers at 1550 nm for both generation and detection. In the THz-TDS setup, a broadband terahertz pulse was generated via optical rectification using a ⟨110⟩ ZnTe crystal. The sample was placed at the focal plane of the terahertz beam, and its

TABLE I. Extracted transport properties from Hall-effect measurements and THz-TDS.

	Hall-effect measurements			THz-TDS			
Sample	μ_{Hall} (cm^2/V s)	n_s (10^{13} cm^{-2})	σ_b^{Hall} (mS)	σ_b^0 (mS)	σ_h^0 (mS)	τ_e (fs)	$\mu_{e,drift}$ (cm^2/V s)
S1a	366	2.81	1.65	1.78 ± 0.09	0.13 ± 0.08	136.80 ± 3.54	1201 ± 31
S1b	250	4.78	1.91	2.15 ± 0.04	0.21 ± 0.12	105.70 ± 6.41	928 ± 56
S1c	359	3.24	1.86	1.85 ± 0.08	0.18 ± 0.10	134.44 ± 4.78	1180 ± 42
S1d	290	3.1	1.44	1.51 ± 0.07	0.24 ± 0.13	122.00 ± 10.66	1071 ± 94
S2	93.7	3.2	0.47	0.90 ± 0.15	0.08 ± 0.03	100.85 ± 4.50	886 ± 40
S3	153	4.31	1.05	1.88 ± 0.16	0.17 ± 0.09	94.28 ± 27.37	828 ± 240

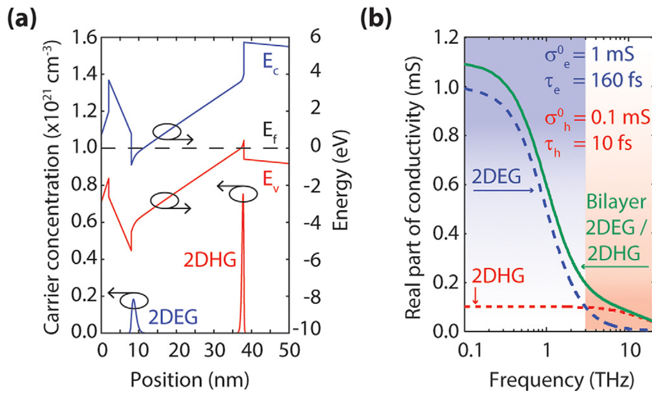

FIG. 2. (a) Self-consistent Schrodinger-Poisson simulation of the electronic structure of the AlN/GaN/AlN QW and calculated charge concentrations at the interfaces. Strong internal polarization fields induce 2DEG and 2DHG layers at the upper and lower interfaces of the well, respectively. (b) Modeled effective bilayer dynamic conductivity for the 2DEG/2DHG system as per Eq. (1).

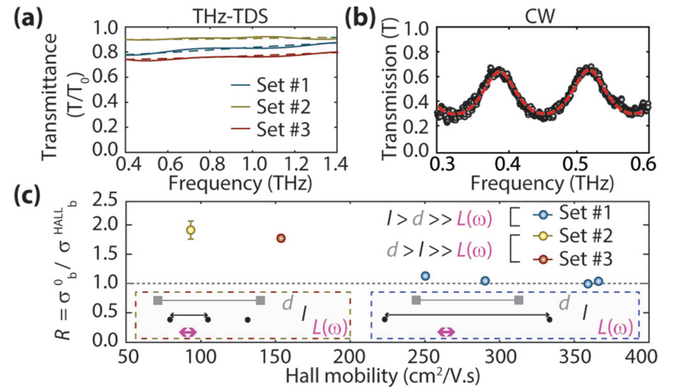

FIG. 3. (a) TDS measurement (continuous lines) and its fit to the model given by Eqs. (2) and (3) (dashed lines) for three representative samples corresponding to *Sample Sets #1*, *#2*, and *#3*. (b) CW terahertz measurement and its fit for a representative sample corresponding to *Sample Set #1*. (c) The ratio (R) between the THz-extracted zero-frequency bilayer conductivity (σ_b^0) and the bilayer DC conductivity obtained from Hall-effect measurements (σ_b^{Hall}) versus Hall mobility for all the analyzed samples. Depicted in the insets are illustrative sketches of the relationships between $L(\omega)$, l, and d for *Sample Set #1* (right inset) and *Sample Sets #2* and *#3* (left inset), where $L(\omega)$ is the characteristic length at which transport is probed by terahertz spectroscopy, d is the characteristic length at which transport is probed in DC measurements, and l is the mean free path between scattering events due to structural effects. The fact that $R > 1$ in *Sample Sets #2* and *#3* is attributed to d, l, and $L(\omega)$, satisfying $d > l > L(\omega)$.

response was modulated using electro-optic sampling in a separate ⟨110⟩ ZnTe detection crystal.[11] The transmitted signal was Fourier transformed to obtain its frequency spectra, which was then normalized by the response of a reference substrate. Data in the 0.4 to 1.6 THz frequency range were obtained from THz-TDS measurements; CW transmission measurements (0.3 to 0.6 THz) were performed so to confirm the low frequency end of the THz-TDS data. The effective bilayer conductivity of the electron/hole system in the GaN QW was experimentally determined by fitting the normalized terahertz transmission (T/T_0) using the following expression:[12]

$$T/T_0 = |1 + Z_0\sigma_b(\omega)/\left(1+\sqrt{\varepsilon_{sub}}\right)|^{-2}, \tag{2}$$

where the transmission (T) through each sample is normalized by that through an appropriate bare reference substrate (T_0); Z_0 is the vacuum impedance ($Z_0 = 377\ \Omega$), and ε_{sub} is the relative permittivity of the substrate, which corresponds to 9.7, 9.3, and 9.1 for samples in *Set* #1 (SiC), #2 (Sapphire), and #3 (AlN), respectively. From Eqs. (1) and (2), the transmission spectrum is expected to exhibit unique spectral signatures arising from the interactions of terahertz waves with different charge carrier species. As shown in Fig. 2(b), electrons and holes depict very distinct spectral behaviors. As a result, two key spectral features are anticipated: (*i*) a rapid extinction drop owing to the long relaxation time characteristic of electrons and (*ii*) a gradual decay as a result of the very short relaxation time of holes.

We can extract several material parameters from the transmission data in the THz-TDS frequency window. By assuming that $\omega\tau_h \ll 1$, which is the case in the 0.4 to 1.6 THz TDS range of operation, Eq. (1) can be reduced to

$$\sigma_b(\omega) = \left(\sigma_b^0 - \sigma_h^0\right)/(1 + j\omega\tau_e) + \sigma_h^0, \tag{3}$$

Therefore, σ_b^0, σ_h^0, and τ_e can be extracted by fitting to the model in Eqs. (2) and (3). In Fig. 3(a), we show the transmission spectra through samples *S1d*, *S2*, and *S3*, as well as their fitting to the model. The extracted bilayer conductivity ($\sigma_b^0 = \sigma_h^0 + \sigma_e^0$) is 1.51 ± 0.07, 0.90 ± 0.15, and 1.88 ± 0.16 mS for samples *S1d*, *S2*, and *S3*, respectively. Moreover, the extracted electron momentum relaxation times are 122.0 ± 10.66, 100.85 ± 4.5, and 94.28 ± 27.37 fs, respectively. Listed in Table I are the extracted values of σ_b^0, σ_h^0, and τ_e for all the analyzed samples. *Because of the limited spectral range in these measurements, a large uncertainty is observed in the extracted hole zero-frequency dynamic conductivity*. Although terahertz spectroscopy enables us to directly extract the conductivity and relaxation times associated with charge carriers, it is also possible to indirectly extract other parameters, such as charge density and mobility, by assuming an appropriate effective mass. By assuming an electron effective mass of $m_e = 0.2m_0$, electron drift mobilities ranging from 828 ± 240 (*Sample S3*) to $1201 \pm 31\ \mathrm{cm^2/V\,s}$ (*Sample S1a*) are extracted across all the analyzed samples. A comparison of these mobility levels with those extracted from Hall measurements requires careful analysis and will be discussed later in the manuscript. Moreover, the corresponding electron densities range from 0.6 ± 0.1 (*Sample S2*) to $1.3 \pm 0.1 \times 10^{13}\ \mathrm{cm^{-2}}$ (*Sample S1b*).

To further validate the measured data, we performed CW terahertz measurements. A representative transmission spectrum, i.e., for sample *S1d*, is depicted in Fig. 3(b). Owing to the presence of Fabry-Perot resonances, the experimental transmission data were fitted to an analytical model based on the transfer-matrix formalism following the methods described in Ref. 13. In Fig. 3(b), we show the calculated transmission spectra that best fit the experimental data, and the extracted zero-frequency bilayer conductivity is 1.48 ± 0.12 mS. This value agrees well with the value obtained from THz-TDS. Overall, an excellent agreement was observed between THz-TDS and CW measurements across all samples.

To qualitatively compare the THz-extracted zero-frequency bilayer conductivity (σ_b^0) with the bilayer DC conductivity obtained from Hall-effect measurements (σ_b^{Hall}), we

computed their ratio ($R = \sigma_b^0/\sigma_b^{Hall}$). Figure 3(c) depicts the computed R for all the analyzed samples. In general, we observe that for samples in *Sample Set #1*, R is close to unity. However, for samples corresponding to *Sample Sets #2 and #3*, the THz-extracted conductivities are up to two-times larger than those extracted from Hall-effect measurements. In this regard, it is worth mentioning that terahertz spectroscopy at a frequency ω probes charge transport in a characteristic length given by $L(\omega) = \sqrt{D/\omega}$, which corresponds to the length-scale that a gas of carriers diffuses before the terahertz electromagnetic fields reverse the direction.[14] As a result, $L(\omega)$ depends on the probe frequency and the diffusion coefficient (D) for charge carriers in the material under test, which ranges in the order of 5–30 cm^2/s for charge carriers in GaN.[15] From this perspective, we find that at terahertz frequencies, i.e., $f > 300$ GHz, the characteristic length is <40 nm. The scale of this characteristic length indicates that the zero-frequency bilayer conductivity extracted from terahertz measurements is a spatially averaged nanoscale conductivity and is thus less affected by microscopic scale effects with a characteristic scattering length of >40 nm than the conductivity extracted from DC Hall-effect measurements. In this regard, the fact that the largest R occurs in samples exhibiting the lowest Hall mobility (i.e., *Sample Sets #2 and #3*) suggests that defects and dislocations present in these sample sets introduce additional scattering with a characteristics length of >40 nm, thus heavily affecting the DC charge transport in these particular samples. This is consistent with previous observations in other materials systems.[16,17] On the other hand, in samples exhibiting the highest Hall mobilities (i.e., *Sample Set #1*) and a unity R, transport is likely limited by other factors with a characteristic length of <40 nm such as interface roughness scattering, phonon scattering, Stark-effect scattering, and interlayer Coulomb drag effects, as discussed in Ref. 5.

Extraction of the relaxation time for the 2DHG requires extending our measurements beyond the THz-TDS frequency window. For this purpose, we performed transmission measurements in the 3 to 14 THz frequency range employing an FTIR system (Bruker IFS-88). Owing to their large size and low substrate surface roughness, two samples from *Sample Set #1* (*S1c* and *S1d*) were analyzed. A representative extinction spectrum (sample *S1d*) is depicted in Fig. 4, which consists of THz-TDS data (0.4 to 1.6 THz) and FTIR data (3 to 14 THz). The upper frequency limit for the FTIR measurement was set to 14 THz in order to remain below the Reststrahlen band corresponding to TO phonons in SiC.[4] The extinction spectra were fitted to the model in Eqs. (1) and (2), from which σ_e^0, τ_e, σ_h^0, and τ_h were extracted. Overall, the measured extinction spectra closely agree with this model as observed in Fig. 4. Furthermore, two different frequency regimes are distinguished, which are correspondingly associated with a short and a long scattering time. The fact that the extinction does not reach zero even at a upper frequency of 14 THz is a signature of free carrier absorption by holes in the 2DHG located at the bottom interface of the QW. The extracted zero-frequency electron conductivity is 1.72 ± 0.04 and 1.32 ± 0.08 mS for samples *S1c* and *S1d*, respectively. The extracted zero-frequency hole conductivities are 0.11 ± 0.05 and 0.19 ± 0.04 mS. Moreover,

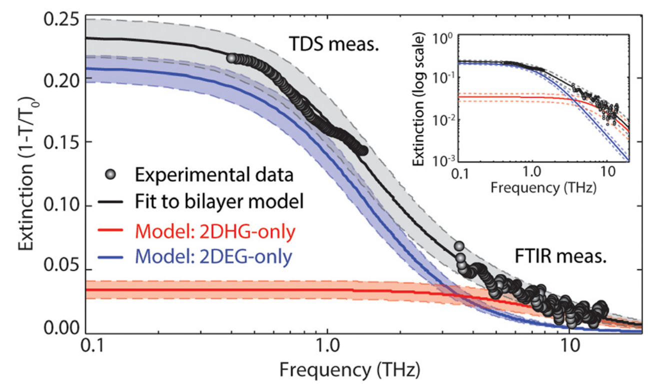

FIG. 4. Representative extinction spectra over an extended frequency range (*Sample #1d*). The data from 0.4 to 1.4 THz were obtained via THz-TDS, while the data from 3 to 14 THz were obtained via FTIR spectroscopy. The continuous black line corresponds to the best fit of the measured data to the analytical model given by Eqs. (1) and (2). For reference, modeled spectral signatures corresponding to a 2DEG-only (blue) and a 2DHG-only (red) exhibiting zero-frequency conductivities and relaxation times consistent with those experimentally extracted for this sample are also shown in the plot. The colored shaded regions located between dashed traces represent uncertainty margins at the 95% confidence level. The inset depicts the same plot on a log-log scale, showing in more detail the fit of the high frequency data to the model.

the extracted electron momentum relaxation times are 155.16 ± 7.44 and 124.72 ± 9.18 fs, and the extracted hole relaxation times are 7.40 ± 4.23 and 19.20 ± 2.81 fs, respectively. *A close agreement is observed between these values, which are obtained from a fitting over an extended frequency spectra, and those extracted only from THz-TDS data*. It is also worth mentioning that the extracted hole momentum relaxation times are in good agreement with those obtained from FTIR spectroscopy of *p*-GaN samples on semi-insulating GaN/SiC (11.8 ± 4.2 fs) (see Fig. S2 in the supplementary material).

From the energy band diagram simulations discussed in the supplementary material, the estimated hole populations in the hole subbands are 4.0×10^{13} cm^{-2} and 0.7×10^{13} cm^{-2} for heavy-holes (HH) and light-holes (LH), respectively; the effective masses for HH and LH correspond to $m_{HH} = 2.11 m_0$ and $m_{LH} = 0.41 m_0$, respectively. By assuming that carriers in both subbands are subjected to similar scattering mechanisms and thus considering similar scattering times for both populations, it is expected that each population will contribute equally to the measured terahertz extinction. Apportioning half of the conductivity to each population and employing the calculated effective mass for each subband, the following hole densities are extracted from the experimental data: $5.51 \pm 2.41 \times 10^{13}$ cm^{-2} (HH) and $1.07 \pm 0.38 \times 10^{13}$ cm^{-2} (LH) and $3.67 \pm 0.79 \times 10^{13}$ cm^{-2} (HH) and $0.71 \pm 0.15 \times 10^{13}$ cm^{-2} (LH), for samples *S1c* and *S1d*, respectively, which are in good agreement with the values predicted from band diagram simulations. Furthermore, from the extracted relaxation times, the following hole mobilities are calculated: 6.17 ± 3.52 cm^2/V s (HH) and 31.70 ± 18.12 cm^2/V s (LH) and 15.98 ± 2.34 cm^2/V s (HH) and 82.25 ± 12 cm^2/V s (LH), for samples *S1c* and *S1d*, respectively.

At this end, since the full-transport properties of the 2DEG and the 2DHG have been extracted, it is possible for us to explain physical reasons behind the modest observed

Hall mobility. This will be attributed to two effects: (*i*) a non-unity Hall-factor and (*ii*) the effect of holes, which due to their considerable contribution to the overall conductivity substantially reduce the apparent Hall mobility. In general, for a multilayer system containing multiple electron and hole layers, the resultant Hall mobility is a weighted average given by

$$\mu_{Hall} = \sum\nolimits_{i\,(electrons)} \mu_i \frac{\sigma_i}{\sigma_{total}} - \sum\nolimits_{j\,(holes)} \mu_j \frac{\sigma_j}{\sigma_{total}}. \quad (4)$$

Across all the analyzed samples, we observe an average electron density of $\sim 1.0 \times 10^{13}\,\mathrm{cm}^{-2}$, an average electron drift mobility of $\sim 1000\,\mathrm{cm}^2/\mathrm{V\,s}$, and an overall contribution of holes to the total conductivity of up to 20%. Using these numbers, and assuming LH and HH mobilities of $\sim 60\,\mathrm{cm}^2/\mathrm{V\,s}$ and $\sim 10\,\mathrm{cm}^2/\mathrm{V\,s}$, respectively, we estimate a weighted mobility of $\sim 790\,\mathrm{cm}^2/\mathrm{V\,s}$, as per Eq. (4). From this perspective, *the smaller Hall-effect mobility observed in experiments is in part a result of holes contributing to the overall conductivity and reducing the apparent Hall mobility*. However, by only accounting for this effect, there is still a significant difference between THz-extracted and Hall-effect extracted mobility levels. For many semiconductors, including GaN, a conversion factor (Hall-factor) is defined to obtain the true carrier concentration from the measured Hall coefficient. This Hall-factor also represents the ratio between Hall mobility and drift mobility ($r_{Hall} = \mu_{Hall}/\mu_{drift}$).[18] An issue when determining the Hall factor is that it is typically not possible to independently extract drift and Hall mobilities under the same experimental conditions. From this point of view, extraction of r_{Hall} often relies on fitting of the Hall mobility versus temperature to theoretical models. However, these methods are adequate at low temperatures and low charge concentrations, where elastic and isotropic scattering processes are dominant.[18] In spite of these limitations, non-unity Hall-factors have been widely reported in the literature, with both $r_{Hall} > 1$ and $r_{Hall} < 1$ depending on dominating scattering mechanisms in the samples.[18–21] In this work, our methodology enabled us to independently extract both μ_{Hall} and μ_{drift} under the same experimental conditions. Based on the estimated weighted mobility, we calculate $r_{Hall} \sim 0.5$ in *Sample Set #1*, which has higher mobilities. This value is consistent with our observations in AlGaN/GaN 2DEGs (see supplementary material) where a Hall mobility of $\sim 1400\,\mathrm{cm}^2/\mathrm{V\,s}$ was observed in spite of a much larger THz-extracted drift mobility of $2000\,\mathrm{cm}^2/\mathrm{V\,s}$ (i.e., $r_{Hall} \sim 0.7$). Investigations on the physical reasons behind these particular extracted values fall out of the scope of this manuscript and will be the subject of future investigations.

In conclusion, we have reported on the terahertz properties of strained AlN/GaN/AlN QWs. Simulations predict that carriers concentrate near the interfaces forming 2D charge gases of distinct carrier species. Using a combination of THz-TDS and FTIR measurements, we were able to individually extract their nanoscale transport properties. Our results evidence that a non-unity Hall-factor and the considerable contribution of holes to the overall conductivity lead to a reduced apparent electron mobility in Hall-effect measurements.

See supplementary material for details on band diagram simulations and terahertz spectroscopy data of control samples.

This work was in part supported by the ONR, MURI N00014-11-1-0721, monitored by Paul Maki and by the AFOSR, FA9550-17-1-0048, monitored by Ken Goretta. This work was also supported by the NSF MRSEC program at the University of Utah, DMR #1121252, and by NSF ECCS #1407959.

[1] S. N. Mohammad, A. A. Salvador, and H. Morkoc, Proc. IEEE **83**(10), 1306 (1995).
[2] F. A. Ponce and D. P. Bour, Nature **386**, 351 (1997).
[3] U. Mishra, S. Likun, T. Kazior, and Y.-F. Wu, Proc. IEEE **96**, 287 (2008).
[4] M. E. Levinshtein and S. L. Rumyantsev, *Properties of Advanced Semiconductor Materials: GaN, AlN, SiC, BN, SiC, SiGe* (John Wiley & Sons, New Jersey, 2001).
[5] M. Qi, G. Li, S. Ganguly, P. Zhao, X. Yan, J. Verma, B. Song, M. Zhu, K. Nomoto, H. G. Xing, and D. Jena, Appl. Phys. Lett. **110**, 063501 (2017).
[6] C. Liu, Y. K. Ooi, S. M. Islam, J. Verma, H. G. Xing, D. Jena, and J. Zhang, Appl. Phys. Lett. **110**, 071103 (2017).
[7] M. Qi, G. Li, V. Protasenko, P. Zhao, J. Verma, B. Song, S. Ganguly, M. Zhu, Z. Hu, X. Yan, A. Mintairov, H. G. Xing, and D. Jena, Appl. Phys. Lett. **106**, 041906 (2015).
[8] W. Zhang, A. K. Azad, and D. Grischkowsky, Appl. Phys. Lett. **82**, 2841 (2003).
[9] B. Sensale-Rodriguez, T. Fang, R. Yan, M. M. Kelly, D. Jena, L. Liu, and H. Xing, Appl. Phys. Lett. **99**, 113104 (2011).
[10] Q. Wei, Z. Wu, K. Sun, F. A. Ponce, J. Hertkorn, and F. Scholz, Appl. Phys. Express **2**, 121001 (2009).
[11] A. Nahata, A. S. Weling, and T. F. Heinz, Appl. Phys. Lett. **69**, 2321 (1996).
[12] M. Tinkham, Phys. Rev. **104**, 845 (1956).
[13] B. Sensale-Rodriguez, R. Yan, M. M. Kelly, T. Fang, K. Tahy, W. S. Hwang, D. Jena, L. Liu, and H. G. Xing, Nat. Commun. **3**, 780 (2012).
[14] P. F. Henning, C. C. Homes, S. Maslov, G. L. Carr, D. N. Basov, B. Nikolić, and M. Strongin, Phys. Rev. Lett. **83**, 4880 (1999).
[15] H. Morkoç, *Handbook of Nitride Semiconductors and Devices* (Wiley-VCH, Weinheim, 2008).
[16] S. Arezoomandan, H. C. Quispe, A. Chanana, P. Xu, A. Nahata, B. Jalan, and B. Sensale-Rodriguez, APL Mater. **4**, 076107 (2016).
[17] J. D. Buron, F. Pizzocchero, B. S. Jessen, T. J. Booth, P. F. Nielsen, O. Hansen, M. Hilke, E. Whiteway, P. U. Jepsen, P. Bøggild, and D. H. Petersen, Nano Lett. **14**, 6348 (2014).
[18] G. Ng, D. Vasileska, and D. K. Schroder, J. Appl. Phys. **106**, 053719 (2009).
[19] R. S. Balmer, K. P. Hilton, K. J. Nash, M. J. Uren, D. J. Wallis, D. Lee, A. Wells, M. Missous, and T. Martin, Semicond. Sci. Technol. **19**, L65 (2004).
[20] D. L. Rode and D. K. Gaskill, Appl. Phys. Lett. **66**, 1972 (1995).
[21] D. C. Look, J. R. Sizelove, S. Keller, Y. F. Wu, U. K. Mishra, and S. P. DenBaars, Solid State Commun. **102**, 297–300 (1997).